

Loop induced $W^\pm H^\mp$ associated production via photon-photon collisions in the THDM and the MSSM *

Zhou Fei^b, Ma Wen-Gan^{a,b}, Jiang Yi^b, Li Xue-Qian^{a,c} and Wan Lang-Hui^b

^a CCAST (World Laboratory), P.O.Box 8730, Beijing 100080, P.R.China

^b Department of Modern Physics, University of Science and Technology of China (USTC), Hefei, Anhui 230027, P.R.China

^c Department of Physics, Nankai University, Tianjin 300070, China

Abstract

We study the loop induced production of charged Higgs boson associated with W-boson via photon-photon collisions at linear colliders (LC). The investigation is carried out under the two-Higgs-doublet model(THDM) and the minimal supersymmetric model (MSSM) using full on-mass-shell renormalization scheme. The numerical analysis of their production rates is presented with some typical parameter sets. The results show that the total cross sections in frame of the MSSM at linear colliders(LC) can reach 0.1 femto barn quantitatively. The contributions from supersymmetric sector can lead to an order of magnitude enhancement of the cross section in some parameter space. We conclude that the associated $W^\pm H^\mp$ production rate in photon-photon collision mode is comparable to that in e^+e^- collision mode.

PACS number(s): 12.60.Jv, 12.60.Fr, 12.15.Lk, 13.85.-t

*The project supported by National Natural Science Foundation of China

1 Introduction

As we know the Higgs sector is one of the essential aspects of the Standard Model(SM) [1][2], responsible for spontaneous symmetry breaking and the generation of masses for the fermions and gauge bosons. But until now the origin of electroweak symmetry breaking has not yet been directly tested by experiments. The extensions of the SM can lead to additional physical Higgs bosons. Particularly the general two-Higgs-doublet model(THDM) and the minimal supersymmetric model(MSSM) [3][4] necessarily involve charged Higgs bosons H^\pm . Because of its electrical charge, the charged Higgs boson is noticeably different from neutral Higgs particles. Therefore, experimental discovery of Higgs bosons including charged Higgs bosons is one of the important goals of the present and future colliders.

Here we review briefly the production mechanisms for charged Higgs bosons at hadron colliders for a comparison between the production mechanisms at LC and at the TeV energy scale hadron colliders, At hadron colliders, there are several mechanisms which can produce charged Higgs bosons[5].

(1) The charged Higgs boson pair can be produced by $q\bar{q} \rightarrow H^+H^-$ [6] and gluon-gluon fusions at one-loop $gg \rightarrow H^+H^-$ [7] at the LHC. Since the heavy H^\pm -bosons decay dominantly into quark pairs, the pair production process is always accompanied by serious QCD backgrounds.

(2) When $m_{H^\pm} < m_t - m_b$, the H^\pm bosons can abundantly be produced in decays of top (anti-top) quarks $t\bar{t} \rightarrow bH^+(\bar{b}H^-)$ from the parent production channel $pp \rightarrow t\bar{t}$. The dominant decay channels in this mass range are $H^+(H^-) \rightarrow \bar{\tau}\nu_\tau(\tau\bar{\nu}_\tau)$.

(3) When $m_{H^\pm} > m_t - m_b$, the single charged Higgs boson production can be via $gb(g\bar{b}) \rightarrow tH^-(\bar{t}H^+)$ [8], $gg \rightarrow t\bar{b}H^-(\bar{t}bH^+)$ [9] and $qb(\bar{q}\bar{b}) \rightarrow q'bH^+(\bar{q}'\bar{b}H^+)$ processes [10]. The sequential decay $H^+ \rightarrow t\bar{b}$ is known as a preferred channel for H^\pm boson search. But signals in these processes appear together with large QCD background. The associated heavy H^\pm production with W boson is another important channel in production of the heavy H^\pm bosons which has been investigated in Refs. [11][12][13]. In this case the W^\pm -boson's leptonic decay may be used as a spectacular trigger.

In the future linear colliders (LC) there are several mechanisms which can produce charged Higgs bosons:

(1) Pair production via $e^+e^- \rightarrow H^+H^-$ and $e^+e^- \rightarrow \gamma\gamma \rightarrow H^+H^-$. The former has already been studied at the tree-level in Ref.[14] and one-loop order in Refs. [15][16]. The latter production process is through laser back-scattered $\gamma\gamma$ collisions and has been studied in Ref.[17]. It is found that these two processes are prominent in discovery of the charged Higgs bosons.

(2) Single production of charged Higgs boson in association with W gauge boson at e^+e^- colliders provides an attractive alternative in searching for H^\pm , which is kinematically favored when m_{H^\pm} exceeds m_W . In Ref.[18] the associated production mechanism via direct e^+e^- collisions has been studied in the THDM. Since there is no tree-level $H^\pm W^\mp V$ couplings ($V = \gamma$ and Z^0), both the $H^\pm W^\mp$ associated production processes via $\gamma\gamma$ and e^+e^- collisions have no tree-level contribution in the THDM and the MSSM and occur at one-loop level in the lowest order.

In this paper we concentrated ourselves on the investigation of the process $e^+e^- \rightarrow \gamma\gamma \rightarrow W^\pm H^\mp$ including the complete contributions in a non-SUSY THDM and the MSSM at LC. Since both the $W^\pm H^\mp$ associated production processes via e^+e^- and laser back-scattered $\gamma\gamma$ collision modes are all one-loop induced at the lowest order, and from the technical point of view there is no problem in realizing the luminosity of laser back-scattered photon beam approaching to that of electron beam, the production rate through $\gamma\gamma$ collisions could be competitive with the e^+e^- colliding mode at LC. We arrange this paper as follows. In Sec.2 we present the analytical calculation. In Sec.3 we give some numerical presentations and discuss the numerical results of the processes $e^+e^- \rightarrow \gamma\gamma \rightarrow W^\pm H^\mp$. In frame of the MSSM we do numerical calculation in the minimal supergravity (mSUGRA) scenario [19]. The conclusions are contained in Sec.IV. Finally some notations used in this paper and the explicit expressions of the self-energies are collected in the Appendix.

2 The Calculation of $e^+e^- \rightarrow \gamma\gamma \rightarrow W^+H^-$

In this section we investigate the process

$$e^+e^- \rightarrow \gamma\gamma \rightarrow W^+H^-$$

in frames of a CP conserving non-SUSY THDM and MSSM. In these models the cross section of $e^+e^- \rightarrow \gamma\gamma \rightarrow W^-H^+$ coincides with the process $e^+e^- \rightarrow \gamma\gamma \rightarrow W^+H^-$ because of the charge conjugation invariance. Our calculation in this section is concentrated on the process $e^+e^- \rightarrow \gamma\gamma \rightarrow W^+H^-$, unless otherwise stated. But the numerical results of the total cross section in Section III involve both two processes i.e. $e^+e^- \rightarrow \gamma\gamma \rightarrow W^\pm H^\mp$. Hence our numerical results of total cross section contain a factor of 2 in contrast to only W^+H^- production.

In our calculation, we adopt the 't Hooft-Feynman gauge, and use dimension regularization scheme for the calculations in frame of the non-SUSY THDM and dimension reduction scheme in frame of the MSSM. We denote the reaction of W^+H^- production via photon-photon collisions as:

$$\gamma(p_1, \mu)\gamma(p_2, \nu) \longrightarrow W^+(k_1, \lambda)H^-(k_2).$$

where p_1 , p_2 and k_1 , k_2 represent the four momenta of the incoming photons and outgoing W^+ and H^- , respectively. The Mandelstam variables are defined as $\hat{s} = (p_1 + p_2)^2$, $\hat{t} = (p_1 - k_1)^2$ and $\hat{u} = (p_1 - k_2)^2$.

We depict the generic Feynman diagrams contributing to the subprocess $\gamma\gamma \rightarrow W^-H^+$ in Fig.1 in the frame of the MSSM. As shown in the figure, this is a one-loop induced subprocess. The diagrams with internal supersymmetric particles \tilde{q} , $\tilde{\chi}^+$ and $\tilde{\chi}^0$ do not appear in the non-SUSY THDM. In Fig.1 there are self-energy, triangle, box and quartic one-loop diagrams as well as the counter-term for the $\gamma - W^+ - H^-$ vertex appearing in t-channel. The corresponding u-channel diagrams are not shown in this figure. The existence of vertex counterterm is due to the fact that this vertex is absent at the tree level, but is UV-divergent at loop contributions. The $\gamma - W^+ - H^-$ vertex counter-term can be visualized in Fig.1(b.1), (b.2). As this subprocess involves non-diagonal gauge propagators, the loop diagrams in Fig.1(a.1-a.19) and the one-loop diagrams in Fig.1(b.3-b.5) are not UV-finite by themselves. Both the mixing $H^+ - W^+$ and $H^+ - G^+$ propagators have to be renormalized to obtain finite physical results. The explicit self-energy one-loop diagrams for mixings of $H^+ - W^+$ and $H^+ - G^+$ are plotted in Fig.2. Since the $H^+ - W^+$ self-energy diagrams on the external W boson have no contribution as a consequence of on-mass-shell W gauge boson, we do not plot them on Fig.1. By using the renormalization

condition as described in Refs. [20] [21], the sum of Higgs tadpole diagrams and tadpole counter-terms vanishes. Therefore, there is no need to consider the tadpole diagrams in the self-energy calculations.

The Higgs sector of a non-SUSY THDM or the MSSM consists of two scalar doublets. In reference [22] the complete set of Feynman rules for the MSSM is given. Here we follow their notations and conventions. We denote the two Higgs doublets as

$$H_1 = \begin{pmatrix} H_1^1 \\ H_1^2 \end{pmatrix} = \begin{pmatrix} (v_1 + \phi_1^0 - i\chi_1^0)/\sqrt{2} \\ -\phi_1^- \end{pmatrix}, \quad H_2 = \begin{pmatrix} H_2^1 \\ H_2^2 \end{pmatrix} = \begin{pmatrix} \phi_2^+ \\ (v_2 + \phi_2^0 + i\chi_2^0)/\sqrt{2} \end{pmatrix}$$

Theoretically, the self-interactions among charged Higgs bosons of two-Higgs-doublet extension models and the gauge bosons are completely determined by local gauge invariance. The kinetic terms read:

$$\begin{aligned} \mathcal{L}_{kin} = & \left[(\vec{\partial}_\mu + ig_1 \frac{Y_{H_1}}{2} B_\mu + ig_2 T^a W_\mu^a) H_1 \right]^\dagger (\vec{\partial}_\mu + ig_1 \frac{Y_{H_1}}{2} B_\mu + ig_2 T^a W_\mu^a) H_1 + \\ & \left[(\vec{\partial}_\mu + ig_1 \frac{Y_{H_2}}{2} B_\mu + ig_2 T^a W_\mu^a) H_2 \right]^\dagger (\vec{\partial}_\mu + ig_1 \frac{Y_{H_2}}{2} B_\mu + ig_2 T^a W_\mu^a) H_2. \end{aligned} \quad (2.1)$$

where T^a are the $SU(2)$ generators. B_μ and W_μ^a denote the $U(1)_Y$ and $SU(2)_L$ gauge fields respectively, and g_1 and g_2 correspond to their relevant coupling constants. Y_{H_i} ($i = 1, 2$) are the hypercharges of Higgs fields. Our one-loop calculation involves $H^+ - W^+$ and $H^+ - G^+$ mixing self-energies and their relevant counterterms. We adopt the on-mass-shell renormalization scheme suggested in Ref.[20] for the extended Higgs doublets. We define that the Higgs fields and vacuum expectation values are renormalized as below:

$$\begin{aligned} H_i & \rightarrow Z_{H_i}^{1/2} H_i \\ v_i & \rightarrow Z_{H_i}^{1/2} (v_i + \delta v_i) = \left(1 + \frac{\delta v_i}{v_i} + \frac{1}{2} \delta Z_{H_i} \right) v_i, \end{aligned} \quad (2.2)$$

hence

$$\frac{\delta \tan \beta}{\tan \beta} = \frac{\delta v_2}{v_2} - \frac{\delta v_1}{v_1} + \frac{1}{2} (\delta Z_{H_2} - \delta Z_{H_1}).$$

We replace of the free parameters and the fields in the kinetic terms of the Lagrangian Eq.(2.1) by the renormalized parameters and fields to obtain corresponding counterterms at the one-loop order in the Lagrangian, then we can read out all the relevant counterterms

for our process. We define the counterterms δZ_{HG} and δZ_{HW} , which behave as if they were the renormalized constants introduced as:

$$\begin{pmatrix} H^\pm \\ G^\pm \end{pmatrix} \rightarrow \begin{pmatrix} Z_{H^\pm} & \delta Z_{HG}^{(1)} \\ \delta Z_{HG}^{(2)} & Z_{G^\pm} \end{pmatrix} \begin{pmatrix} H^\pm \\ G^\pm \end{pmatrix}, \quad (2.3)$$

and

$$W_\mu^\pm \rightarrow (Z_2^W)^{1/2} W_\mu^\pm \pm i \frac{\delta Z_{HW}}{m_W} \partial_\mu H^\pm, \quad (2.4)$$

where $Z_2^W = 1 + \delta Z_2^W$ is the usual $SU(2)_L$ gauge triplet renormalization constant. Then we get the relations

$$\begin{aligned} \delta Z_{HG}^{(1),(2)} &= \frac{\sin 2\beta}{2} \left[\frac{1}{2} (\delta Z_{H_2} - \delta Z_{H_1}) \mp \frac{\delta \tan \beta}{\tan \beta} \right], \\ \delta Z_{HG} &= \delta Z_{GH}^{(1)} + \delta Z_{HG}^{(2)} = \frac{\sin 2\beta}{2} (\delta Z_{H_2} - \delta Z_{H_1}), \\ \delta Z_{HW} &= \delta Z_{HG}^{(2)}. \end{aligned} \quad (2.5)$$

And the counterterm for the γWH vertex appearing in Fig.1(b.1,b.2) has the form as

$$\delta V_{\gamma WH} = i e g_{\mu\nu} m_W \delta Z_{HG}^{(2)}, \quad (2.6)$$

which is obtained with the above replacement of the Lagragian terms $\mathcal{L} = e m_W A^\mu W_\mu^- G^+ + \text{h.c.} + \dots$ in Eq.(2.1).

Denoting the bare self-energy as Σ , the renormalized one is defined as $\hat{\Sigma} = \Sigma - \delta\Sigma$. Here we define the renormalized two-point Green functions for the $H^+ - W^+$ and $H^+ - G^+$ mixings as

$$\begin{aligned} G_\mu^{HW} &= \frac{-i}{p^2 - m_{H^\pm}^2} p^\nu (\Sigma_{HW} - \delta\Sigma_{HW}) \frac{-i g_{\mu\nu}}{p^2 - m_W^2}, \\ G^{HG} &= \frac{-i}{p^2 - m_{H^\pm}^2} (\Sigma_{HG} - \delta\Sigma_{HG}) \frac{i}{p^2 - m_W^2}, \end{aligned}$$

respectively. The counterterm $\delta\Sigma$ can be derived from the bare self-energy expression by using on-mass-shell scheme. With an on-mass-shell charged Higgs boson, the real part of the renormalized mixing self-energy $\hat{\Sigma}_{HW}|_{p^2=m_{H^\pm}^2}$ should be zero, i.e.

$$\text{Re} \hat{\Sigma}_{HW}|_{p^2=m_{H^+}^2} = 0 \implies \delta Z_{HW} = \frac{\text{Re} \Sigma_{HW}(m_{H^\pm}^2)}{m_W^2}. \quad (2.7)$$

For the renormalized self-energies $\hat{\Sigma}_{HW}$ and $\hat{\Sigma}_{HG}$, we have the Slavnov-Taylor identity [23]

$$k^2 \hat{\Sigma}_{HW}(p^2) - m_W \hat{\Sigma}_{HG}(p^2) = 0, \quad \text{at } p^2 = m_{H^+}^2. \quad (2.8)$$

From the above two equations we can get

$$Re \hat{\Sigma}_{HG}|_{p^2=m_{H^+}^2} = 0. \quad (2.9)$$

Then we obtain the related counterterms of the self-energies as

$$\begin{aligned} \delta \Sigma_{HW} &= Re \Sigma_{HW}|_{p^2=m_{H^+}^2} = Re(\Sigma_{HW}^f + \Sigma_{HW}^b)|_{p^2=m_{H^+}^2}, \\ \delta \Sigma_{HG} &= Re \Sigma_{HG}|_{p^2=m_{H^+}^2} = Re(\Sigma_{HG}^f + \Sigma_{HG}^b)|_{p^2=m_{H^+}^2}, \end{aligned} \quad (2.10)$$

where $\Sigma_{HW,HG}^f$ and $\Sigma_{HW,HG}^b$ denote the unrenormalized self-energy parts from the fermion loop and boson loop diagrams, respectively. The unrenormalized self-energies Σ_{HW} and Σ_{HG} can be calculated from the diagrams in Fig.2. Due to the on-mass-shell renormalization condition, the quartic self-energy diagrams in Fig.2(5) does not contribute to the $H^+ - G^+$ self-energy.

Since the incoming photons are unpolarized, it is required to average over their polarization. The sum of the photon polarization vector $\epsilon^\mu(\lambda_1, p_1)$ and $\epsilon^\nu(\lambda_2, p_2)$ has to be chosen in such a way that only the physical(transverse) polarization states remain and the unphysical one(longitudinal) does not contribute to matrix element[24]:

$$\sum_{\lambda=1,2} \epsilon^{\mu*}(\lambda, p) \epsilon^\nu(\lambda, p) = -g^{\mu\nu} + 2 \frac{p_1^\mu p_2^\nu + p_1^\nu p_2^\mu}{\hat{s}}, \quad (p = p_1, p_2). \quad (2.11)$$

The renormalized amplitude of the subprocess is expressed as

$$\begin{aligned} \mathcal{M} &= \mathcal{M}_{(t)}^{\text{loop}} + \mathcal{M}_{(t)}^{\text{ct}} + \mathcal{M}_{(t)}^{\text{bub}} + \mathcal{M}_{(u)}^{\text{loop}} + \mathcal{M}_{(u)}^{\text{ct}} + \mathcal{M}_{(u)}^{\text{bub}} \\ &= \epsilon^\mu(p_1) \epsilon^\nu(p_2) \epsilon^\lambda(-k_1) (f_1 g_{\mu\nu} p_{2\lambda} + f_2 g_{\mu\nu} p_{1\lambda} + f_3 g_{\mu\lambda} k_{1\nu} + f_4 g_{\nu\lambda} k_{1\mu} + f_5 k_1^\alpha \epsilon_{\alpha\mu\nu\lambda} \\ &\quad + f_6 p_1^\alpha \epsilon_{\mu\nu\lambda\alpha} + f_7 p_2^\alpha \epsilon_{\mu\nu\lambda\alpha} + f_8 k_{1\mu} k_{1\nu} p_{2\lambda} + f_9 k_{1\mu} k_{1\nu} p_{1\lambda} + f_{10} k_1^\alpha p_1^\beta p_{2\lambda} \epsilon_{\alpha\mu\nu\beta} \\ &\quad + f_{11} k_1^\alpha p_2^\beta p_{2\lambda} \epsilon_{\alpha\mu\nu\beta} + f_{12} k_1^\alpha p_{1\lambda} p_2^\beta \epsilon_{\alpha\mu\nu\beta} + f_{13} k_1^\alpha k_{1\nu} p_1^\beta \epsilon_{\alpha\mu\lambda\beta} + f_{14} k_1^\alpha p_2^\beta k_{1\nu} \epsilon_{\alpha\mu\lambda\beta} \\ &\quad + f_{15} k_1^\alpha p_2^\beta k_{1\mu} \epsilon_{\alpha\nu\lambda\beta} + f_{16} p_1^\alpha p_2^\beta p_{2\lambda} \epsilon_{\mu\nu\alpha\beta} + f_{17} p_1^\alpha p_2^\beta p_{1\lambda} \epsilon_{\mu\nu\alpha\beta} + f_{18} k_{1\nu} p_1^\alpha p_2^\beta \epsilon_{\mu\lambda\alpha\beta} \\ &\quad + f_{19} k_{1\mu} p_1^\alpha p_2^\beta \epsilon_{\nu\lambda\alpha\beta} + f_{20} k_1^\alpha p_1^\beta p_2^\gamma \epsilon_{\alpha\mu\beta\gamma} g_{\nu\lambda} + f_{21} k_1^\alpha p_1^\beta p_2^\gamma \epsilon_{\alpha\nu\beta\gamma} g_{\mu\lambda} \\ &\quad + f_{22} k_1^\alpha p_1^\beta p_2^\gamma \epsilon_{\alpha\lambda\beta\gamma} g_{\mu\nu}) = \epsilon^\mu(p_1) \epsilon^\nu(p_2) \epsilon^\lambda(-k_1) \sum_{i=1}^{22} f_i \mathcal{L}_i, \end{aligned}$$

where $f_i (i = 1, 22)$ are the form factors and \mathcal{L}_i are their respective Lorentz tensors. The u-channel matrix parts $\mathcal{M}_{(u)}^{\text{loop}}$, $\mathcal{M}_{(u)}^{\text{ct}}$ and $\mathcal{M}_{(u)}^{\text{bub}}$ are obtained by the following replacements:

$$\begin{aligned}\mathcal{M}_{(u)}^{\text{loop}} &= \mathcal{M}_{(t)}^{\text{loop}}(t \rightarrow u, \mu \leftrightarrow \nu, p_1 \leftrightarrow p_2), \\ \mathcal{M}_{(u)}^{\text{ct}} &= \mathcal{M}_{(t)}^{\text{ct}}(t \rightarrow u, \mu \leftrightarrow \nu, p_1 \leftrightarrow p_2), \\ \mathcal{M}_{(u)}^{\text{bub}} &= \mathcal{M}_{(t)}^{\text{bub}}(t \rightarrow u, \mu \leftrightarrow \nu, p_1 \leftrightarrow p_2),\end{aligned}$$

The amplitude parts of $\mathcal{M}_{(t),(u)}^{\text{loop}}$, $\mathcal{M}_{(t),(u)}^{\text{ct}}$ and $\mathcal{M}_{(t),(u)}^{\text{bub}}$ represent the contributions from the one-loop diagrams Fig.1(a.1-a.19), the counter term diagrams Fig.1(b.1-b.2) and the self-energy bubble diagrams Fig.1(b.3-b.5), respectively. We decompose the amplitude parts of $\mathcal{M}_{(t)}^{\text{ct}}$ and $\mathcal{M}_{(t)}^{\text{bub}}$ as:

$$\begin{aligned}\mathcal{M}_{(t)}^{\text{ct}} &= \mathcal{M}_{b1}^{(t)} + \mathcal{M}_{b2}^{(t)}, \\ \mathcal{M}_{(t)}^{\text{bub}} &= \mathcal{M}_{b3}^{(t)} + \mathcal{M}_{b4}^{(t)} + \mathcal{M}_{b5}^{(t)}.\end{aligned}\tag{2.12}$$

where

$$\begin{aligned}\mathcal{M}_{b1}^{(t)} &= \epsilon^\mu(p_1)\epsilon^\nu(p_2)\epsilon^\lambda(-k_1)\frac{2e\delta V_{\gamma WH}}{\hat{t} - m_{H^+}^2}\mathcal{L}_3 \\ \mathcal{M}_{b2}^{(t)} &= \epsilon^\mu(p_1)\epsilon^\nu(p_2)\epsilon^\lambda(-k_1)\frac{e\delta V_{\gamma WH}}{\hat{t} - m_W^2}(2\mathcal{L}_2 - \mathcal{L}_3 + 2\mathcal{L}_4) \\ \mathcal{M}_{b3}^{(t)} &= \epsilon^\mu(p_1)\epsilon^\nu(p_2)\epsilon^\lambda(-k_1)\frac{2ie^2m_W}{(\hat{t} - m_W^2)(\hat{t} - m_{H^+}^2)}\left(\hat{\Sigma}_{GW} + m_W\hat{\Sigma}_{HW}\right)\mathcal{L}_3 \\ \mathcal{M}_{b4}^{(t)} &= \epsilon^\mu(p_1)\epsilon^\nu(p_2)\epsilon^\lambda(-k_1)\frac{ie^2m_W}{(\hat{t} - m_W^2)(m_{H^+}^2 - m_W^2)} \cdot \\ &\quad \left\{\hat{\Sigma}_{GW}(2\mathcal{L}_2 + \mathcal{L}_3 + 2\mathcal{L}_4) + \hat{\Sigma}_{HW}\left[2m_W\mathcal{L}_3 + \frac{\hat{t}}{m_W}(2\mathcal{L}_2 - \mathcal{L}_3 + 2\mathcal{L}_4)\right]\right\} \\ \mathcal{M}_{b5}^{(t)} &= \epsilon^\mu(p_1)\epsilon^\nu(p_2)\epsilon^\lambda(-k_1)\frac{-ie^2\hat{\Sigma}_{HW}}{m_{H^+}^2 - m_W^2}(2\mathcal{L}_1 + 2\mathcal{L}_2 + \mathcal{L}_3 + \mathcal{L}_4),\end{aligned}$$

The explicit expressions of the related unrenormalized self-energies are listed in Appendix.

The cross section for the subprocess at one-loop order with the unpolarized photon collisions can be obtained from

$$\hat{\sigma}(\hat{s}, \gamma\gamma \rightarrow W^+H^-) = \frac{1}{16\pi\hat{s}^2} \int_{\hat{t}^-}^{\hat{t}^+} d\hat{t} \sum |\mathcal{M}|^2.\tag{2.13}$$

In above equation, we define $\hat{t}^\pm = \left[(m_H^2 + m_W^2 - \hat{s}) \pm \sqrt{(m_H^2 + m_W^2 - \hat{s})^2 - 4m_H^2 m_W^2} \right] / 2$. The bar over the sum means average over initial spins.

With the integrated photon luminosity in the e^+e^- collision, the total cross section of the process $e^+e^- \rightarrow \gamma\gamma \rightarrow W^+H^-$ can be written as:

$$\sigma(s) = \int_{E_0/\sqrt{\hat{s}}}^{x_{max}} dz \frac{d\mathcal{L}_{\gamma\gamma}}{dz} \hat{\sigma}(\gamma\gamma \rightarrow W^+H^- \text{ at } \hat{s} = z^2 s) \quad (2.14)$$

with $E_0 = m_W + m_{H^+}$, and $\sqrt{s}(\sqrt{\hat{s}})$ being the $e^+e^- (\gamma\gamma)$ center-of-mass energy. $d\mathcal{L}_{\gamma\gamma}/dz$ is defined as:

$$\frac{d\mathcal{L}_{\gamma\gamma}}{dz} = 2z \int_{z^2/x_{max}}^{x_{max}} \frac{dx}{x} F_{\gamma/e}(x) F_{\gamma/e}(z^2/x). \quad (2.15)$$

For the initial unpolarized electrons and laser photon beams, the energy spectrum of the back-scattered is given by[25][26][27]

$$F_{\gamma/e} = \frac{1}{D(\xi)} \left[1 - x + \frac{1}{1-x} - \frac{4x}{\xi(1-x)} + \frac{4x^2}{\xi^2(1-x)^2} \right], \quad (2.16)$$

where

$$\begin{aligned} D(\xi) &= \left(1 - \frac{4}{\xi} - \frac{8}{\xi^2}\right) \ln(1 + \xi) + \frac{1}{2} + \frac{8}{\xi} - \frac{1}{2(1 + \xi)^2} \\ \xi &= 4E_0\omega_0/m_e^2, \end{aligned} \quad (2.17)$$

m_e and E_0 are the mass and energy of the electron respectively, and ω_0 is the laser-photon energy, x represents the fraction of the energy of the incident electron carried by the back-scattered photon. In our evaluation, we choose ω_0 such that it maximizes the backscattered photon energy without spoiling the luminosity through e^+e^- pair creation. Then we have $\xi = 2(1 + \sqrt{2}) \simeq 4.8$, $x_{max} \simeq 0.83$ and $D(\xi) \simeq 1.8$.

3 Numerical results and discussions

In this section, we present some numerical results of the total cross section for the processes $e^+e^- \rightarrow \gamma\gamma \rightarrow W^\pm H^\mp$. The SM input parameters are chosen as: $m_t = 174.3 \text{ GeV}$, $m_Z = 91.1882 \text{ GeV}$, $m_b = 4.4 \text{ GeV}$, $\sin^2 \theta_W = 0.23117$, and $\alpha_{EW} = 1/128$ [28].

We take the MSSM parameters in the frame of the mSUGRA scenario. Of the five input parameters (m_0 , $m_{1/2}$, A_0 , $\tan \beta$ and sign of μ) in this theory, we take $m_{1/2}=120$

GeV, $A_0=300$ GeV, $\mu > 0$ and set $\tan \beta$ to typical values. m_0 is tuned to obtain desired m_{H^\pm} which fall in the experimentally constrained range.

In the numerical evaluation for the THDM case, we adopted the following MSSM Higgs mass relations considering the radiative corrections to fix the neutral Higgs boson masses and the mixing angle α [29].

$$\tan 2\alpha = \tan 2\beta \frac{m_A^2 + m_Z^2}{m_A^2 - m_Z^2 + \epsilon / \cos(2\beta)}, \quad \text{where } m_A^2 = m_{H^\pm}^2 - m_W^2, \quad (3.1)$$

$$m_{H^0, h^0}^2 = \frac{1}{2} \left[m_{AZ}^2 \pm \sqrt{m_{AZ}^4 - 4m_Z^2 m_A^2 \cos^2 2\beta - 4\epsilon(m_A^2 \sin^2 \beta + m_Z^2 \cos^2 \beta)} \right] \quad (3.2)$$

with

$$\epsilon = \frac{3G_F}{\sqrt{2}\pi^2} \frac{m_t^4}{\sin^2 \beta} \log \left[\frac{m_{\tilde{t}_L} m_{\tilde{t}_R}}{m_t^2} \right], \quad (3.3)$$

where the left-handed and right-handed scale top-quark masses are determined by formulas in a grand unified (GUT) framework [30]

$$\begin{aligned} m_{\tilde{t}_L}^2 &= m_0^2 + \left(\frac{1}{2} - \frac{2}{3}s_W^2 \right) \cos 2\beta m_Z^2 + m_t^2, \\ m_{\tilde{t}_R}^2 &= m_0^2 + \frac{2}{3}s_W^2 \cos 2\beta m_Z^2 + m_t^2, \end{aligned} \quad (3.4)$$

where at the Plank mass scale we assumed $M_Q^2 = M_U^2 = M_D^2 = m_0^2$. That is to say in the THDM case we take the charged Higgs mass m_{H^\pm} , m_0 and $\tan \beta$ as input parameters and put their quantities being the same as the corresponding ones in the MSSM case when they are allowed in the mSUGRA parameter space, so as to make comparison of the results from both models. We noticed also that there are some charged Higgs mass regions in our plots which are not covered by the allowed parameter space in the mSUGRA scenario (e.g. the dashed lines for the THDM in Fig.3 where $\tan \beta = 2$, $100 \text{ GeV} \leq m_{H^\pm} \leq 300 \text{ GeV}$, and $m_{H^\pm} = 200 \text{ GeV}$, $2 \leq \tan \beta \leq 4$ in Fig.4a, et cetera), there we take $m_0 = 220 \text{ GeV}$. Actually our evaluation shows that by adopting mSUGRA parameters and Eqs.(3.1~3.4) for the MSSM and THDM models respectively, we can get the corresponding neutral Higgs masses and mixing angle α with approximately same quantities in both models. To illustrate this point, we list parameter quantities of neutral Higgs masses and mixing angle α with $\tan \beta = 6$ used in our calculations for both THDM and MSSM models in table 1.

Table 1 The comparison of the corresponding parameter values in the THDM and MSSM with $\tan \beta = 6$

(the MSSM values from the mSUGRA/the THDM values from Eqs.(3.1~3.4))

$m_{H^\pm} [GeV]$	$m_{h^0} [GeV]$	$m_{H^0} [GeV]$	$m_{A^0} [GeV]$	α
210	98.50/96.54	197.40/197.12	194.60/193.99	-0.2547/-0.2644
300	100.10/97.45	291.09/290.83	289.30/289.02	-0.2007/-0.2039
450	102.09/97.80	444.06/443.86	442.75/442.76	-0.1799/-0.1807
550	103.25/97.88	545.15/544.98	543.95/544.09	-0.1750/-0.1753

Fig.3 displays the integrated total cross section of $W^\pm H^\mp$ production at LC with $\sqrt{s} = 1 \text{ TeV}$ versus the mass of H^\pm with $\tan \beta = 2, 6, 32$, respectively. There we can see the sophisticated structures on the MSSM curves, which are induced mainly by the threshold effects from Yukawa couplings of charged Higgs boson to quarks and scalar quarks, at the vicinities where $m_{H^+} = m_{\tilde{t}_i} + m_{\tilde{b}_i}$ ($i=1,2$) and $m_{H^+} = m_t + m_b$ from loop diagrams[13]. It is obvious that the supersymmetric particles in loop can enhance the cross sections of the subprocess substantially by one order. When the ratio of the vacuum expectation values has a small value and the charged Higgs boson mass is in the mediate range, the cross sections of the subprocess can reach 10^{-1} femto barn. Since in the case of the MSSM we use the mSUGRA senario, while in the THDM we use another parameter setting methode mentioned above, some parts of parameter space with small m_{H^+} and $\tan \beta$ in the THDM are not allowed in the mSUGRA parameter sapce. That is why we see in Fig.3 that the curves for the MSSM are not plotted at the lower end.

We present the cross sections of $W^\pm H^\mp$ productions at LC versus $\tan \beta$ in Fig.4a and Fig4.b for a non-SUSY THDM and the MSSM, respectively. Fig.4a is for $\sqrt{s} = 1 \text{ TeV}$, the $\tan \beta$ is in the range of $2 - 35$ and the mass of the charged Higgs boson is taken as 200 GeV , 400 GeV and 600 GeV , respectively. The Fig.4a shows that the cross sections are reduced with the increment of the charged Hoggs boson mass in both models. In Fig.4a, we can see that when the charged Higgs boson has the mass value about 200 GeV and $\sqrt{s} = 1 \text{ TeV}$, the cross sections at LC are in the order of 10^{-2} femto barn in the MSSM THDM and in the range of $10^{-3} - 10^{-2}$ femto barn in the non-SUSY THDM. Fig.4b is for $\sqrt{s} = 500 \text{ GeV}$ and the mass of the charged Higgs boson is chosen as 200 GeV . The two curves correspond to the results for the non-SUSY THDM and the MSSM. All these curves in Fig.4a and Fig.4b show that the cross section is a obviously effected by $\tan \beta$.

That is because the couplings of Higgs bosons to quark(squark) pairs are related to the ratio of the vacuum expectation values. We can see from these figures that the dependence of the cross section on $\tan\beta$ in the MSSM is weaker than in the non-SUSY THDM and the maximal enhancement occurs at the low $\tan\beta$ range. We compared our results in the non-SUSY THDM with those in Ref.[18] and find that the production rates via $\gamma\gamma$ collision mode are of the same order as those via e^+e^- collision mode at LC.

4 Conclusion

In this paper, we study the loop induced W^\pm -associated production of charged Higgs bosons via photon-photon fusion at linear colliders in the non-SUSY THDM as well as in the MSSM. Numerical analysis of their production rates is carried out at one-loop order with some typical parameter sets. With our input parameters, the contributions from SUSY sector can lead to an order of magnitude enhancement of the cross section for the case of the THDM in some parameter space. Our results demonstrate that this production rate via photon-photon collisions at LC can reach about 0.1 femto barn in frame of the MSSM at LC when $m_{H^\pm} \sim 200 \text{ GeV}$. We find that the $H^\pm W^\mp$ -associated production rate via $\gamma\gamma$ collisions at LC is quantitatively comparable to that via the electron-positron collision mode[18].

Acknowledgement:

This work was supported in part by the National Natural Science Foundation of China(project numbers: 19875049, 10005009), a grant from the Education Ministry of China and the State Commission of Science and Technology of China. The authors would like to thank Dr. Zhang Ren-You for helpful discussions.

Appendix

The Feynman rules we used for the couplings can be found in [4]. We denote the couplings concerned in this work as:

$$V_{B+tb} = V_{Btb}^L P_L + V_{Btb}^R P_R,$$

$$\begin{aligned}
V_{B^+\tilde{t}_i\tilde{b}_j} &= V_{B\tilde{t}_i\tilde{b}_j}^L P_L + V_{B\tilde{t}_i\tilde{b}_j}^R P_R, \\
V_{B^+\tilde{\chi}_i^0\tilde{\chi}_j^+} &= V_{B\tilde{\chi}_i^0\tilde{\chi}_j^+}^L P_L + V_{B\tilde{\chi}_i^0\tilde{\chi}_j^+}^R P_R \quad (B^+ = H^+, G^+).
\end{aligned}$$

In our calculation there are several hundred loop diagrams contributing to the sub-process $\gamma\gamma \rightarrow W^\pm H^\mp$. We find their explicit expressions of one-loop diagrams are too complicated and over lengthy to list here. Therefore, we list only the unrenormalized self-energies expressions of mixing $H^+ - W^-$ and $H^+ - G^-$ explicitly in appendix. Their fermion and boson parts are expressed as below:

$$\begin{aligned}
\Sigma_{HW}^f(p^2) &= -\frac{3igd}{32\sqrt{2}\pi^2} \left[m_t V_{Htb}^L B_0[p, m_t, m_b] + (m_t V_{Htb}^L + m_b V_{Htb}^R) B_1[p, m_t, m_b] \right] \\
&+ \sum_{i=1,2}^{j=1-4} \frac{1}{8\pi^2} \left\{ B_0[p, m_{\chi_j^0}, m_{\chi_i^+}] m_{\chi_j^0} (V_{H\tilde{\chi}_j^0\tilde{\chi}_i^+}^{L*} V_{W\tilde{\chi}_j^0\tilde{\chi}_i^+}^L + V_{H\tilde{\chi}_j^0\tilde{\chi}_i^+}^{R*} V_{W\tilde{\chi}_j^0\tilde{\chi}_i^+}^R) \right. \\
&+ B_1[p, m_{\chi_j^0}, m_{\chi_i^+}] \left[V_{H\tilde{\chi}_j^0\tilde{\chi}_i^+}^{L*} (m_{\chi_j^0} V_{W\tilde{\chi}_j^0\tilde{\chi}_i^+}^L + m_{\chi_i^+} V_{W\tilde{\chi}_j^0\tilde{\chi}_i^+}^R) \right. \\
&+ \left. \left. V_{H\tilde{\chi}_j^0\tilde{\chi}_i^+}^{R*} (m_{\chi_i^+} V_{W\tilde{\chi}_j^0\tilde{\chi}_i^+}^L + m_{\chi_j^0} V_{W\tilde{\chi}_j^0\tilde{\chi}_i^+}^R) \right] \right\} \\
\Sigma_{HW}^b(p^2) &= \frac{igV_{H^+G^-h^0}}{32\pi^2} (B_0[p, m_{h^0}, m_W] + 2B_1[p, m_{h^0}, m_W]) \sin(\alpha - \beta) \\
&- \frac{igV_{H^+G^-H^0}}{32\pi^2} (B_0[p, m_{H^0}, m_W] + 2B_1[p, m_{H^0}, m_W]) \cos(\alpha - \beta) \\
&- \frac{igV_{H^+H^-h^0}}{32\pi^2} (B_0[p, m_{h^0}, m_{H^+}] + 2B_1[p, m_{h^0}, m_{H^+}]) \cos(\alpha - \beta) \\
&+ \frac{igV_{WWH^0}}{32\pi^2} (B_0[p, m_{h^0}, m_W] - B_1[p, m_{h^0}, m_W]) \cos(\alpha - \beta) \\
&- \frac{igV_{H^+H^-H^0}}{32\pi^2} (B_0[p, m_{H^0}, m_{H^+}] + 2B_1[p, m_{H^0}, m_{H^+}]) \sin(\alpha - \beta) \\
&- \frac{m_W g^2}{64\pi^2} (B_0[p, m_{H^0}, m_W] - B_1[p, m_{H^0}, m_W]) \sin 2(\alpha - \beta) \\
&- \sum_{i,j=1-2} \left[\frac{3}{16\pi^2} B_0[p, m_{\tilde{t}_j}, m_{\tilde{b}_i}] V_{H\tilde{t}_j\tilde{b}_i} V_{W\tilde{b}_i\tilde{t}_j} + \frac{3}{8\pi^2} B_1[p, m_{\tilde{t}_j}, m_{\tilde{b}_i}] V_{H\tilde{t}_j\tilde{b}_i} V_{W\tilde{b}_i\tilde{t}_j} \right] \\
\Sigma_{HG}^f(p^2) &= 3d \left\{ -A_0[m_b] (V_{Htb}^L V_{Gtb}^{L*} + V_{Htb}^R V_{Gtb}^{R*}) + p^2 B_1[p, m_t, m_b] (V_{Htb}^L \cdot \right. \\
&V_{Gtb}^{L*} + V_{Htb}^R V_{Gtb}^{R*}) + m_t B_0[p, m_t, m_b] (m_t V_{Htb}^L V_{Gtb}^{L*} + m_b \cdot \\
&V_{Htb}^R V_{Gtb}^{L*} + m_b V_{Htb}^L V_{Gtb}^{R*} + m_t V_{Htb}^R V_{Gtb}^{R*}) \left. \right\} / (32\pi^2) \\
&- \sum_{i=1,2}^{j=1-4} \left\{ A_0[m_{\chi_i^+}] (V_{H\tilde{\chi}_j^0\tilde{\chi}_i^+}^{L*} V_{G\tilde{\chi}_j^0\tilde{\chi}_i^+}^L + V_{H\tilde{\chi}_j^0\tilde{\chi}_i^+}^{R*} V_{G\tilde{\chi}_j^0\tilde{\chi}_i^+}^R) \right.
\end{aligned}$$

$$\begin{aligned}
& -p^2 B_1[p, m_{\chi_j^0}, m_{\chi_i^+}](V_{H\tilde{\chi}_j^0\tilde{\chi}_i^+}^{L*} V_{G\tilde{\chi}_j^0\tilde{\chi}_i^+}^L + V_{H\tilde{\chi}_j^0\tilde{\chi}_i^+}^{R*} V_{G\tilde{\chi}_j^0\tilde{\chi}_i^+}^R) \\
& -B_0[p, m_{\chi_j^0}, m_{\chi_i^+}]m_{\chi_j^0} \left[V_{H\tilde{\chi}_j^0\tilde{\chi}_i^+}^{L*} (m_{\chi_j^0} V_{G\tilde{\chi}_j^0\tilde{\chi}_i^+}^L + m_{\chi_i^+} V_{G\tilde{\chi}_j^0\tilde{\chi}_i^+}^R) \right. \\
& \left. + V_{H\tilde{\chi}_j^0\tilde{\chi}_i^+}^{R*} (m_{\chi_i^+} V_{G\tilde{\chi}_j^0\tilde{\chi}_i^+}^L + m_{\chi_j^0} V_{G\tilde{\chi}_j^0\tilde{\chi}_i^+}^R) \right] / (8\pi^2) \\
\Sigma_{HG}^b(p^2) = & (V_{H^+G^-h^0} V_{H^+H^-h^0} B_0[p, m_{h^0}, m_{H^+}]) / (16\pi^2) \\
& + (V_{G^+G^-h^0} V_{H^+G^-h^0} B_0[p, m_{h^0}, m_W]) / (16\pi^2) \\
& + (V_{H^+G^-H^0} V_{H^+H^-H^0} B_0[p, m_{H^0}, m_{H^+}]) / (16\pi^2) \\
& + (V_{G^+G^-H^0} V_{H^+G^-H^0} B_0[p, m_{H^0}, m_W]) / (16\pi^2) \\
& - \left\{ g^2 \left[m_{H^+}^2 (B_0[p, m_{h^0}, m_W] - 2B_1[p, m_{h^0}, m_W] + B_{21}[p, m_{h^0}, m_W]) \right. \right. \\
& \left. \left. - dB_{22}[p, m_{h^0}, m_W] \right] \sin 2(\alpha - \beta) \right\} / (128\pi^2) \\
& + \left\{ g^2 \left[m_{H^+}^2 (B_0[p, m_{H^0}, m_W] - 2B_1[p, m_{H^0}, m_W] + B_{21}[p, m_{H^0}, m_W]) \right. \right. \\
& \left. \left. - dB_{22}[p, m_{H^0}, m_W] \right] \sin 2(\alpha - \beta) \right\} / (128\pi^2) \\
& - 3 \sum_{i,j=1-2} B_0[p, m_{\tilde{t}_j}, m_{\tilde{b}_i}] V_{G\tilde{b}_j\tilde{t}_i}^* V_{H\tilde{t}_j\tilde{b}_i} / (16\pi^2).
\end{aligned}$$

In case of the non-SUSY THDM, we take away the contributions from supersymmetric particles, i.e. scalar quarks and charginos/neutralinos, and used dimensional regularization ($d = 4 - \epsilon$) instead of dimensional reduction ($d=4$). As a check of our results, we find from our calculation that the amplitude of all the diagrams in Fig.1 is UV-finite by themselves. The above self-energy expressions for the non-SUSY THDM do not contradict with those in Ref.[18].

In the above expressions we adopt the definitions of one-loop integral functions in reference [31]. The numerical calculation of the vector and tensor loop integral functions can be traced back to four scalar loop integrals A_0 , B_0 , C_0 , D_0 as shown in [32].

References

- [1] S.L. Glashow, Nucl. Phys. 22 (1961)579; S. Weinberg, Phys. Rev. Lett. 1 (1967)1264; A. Salam, Proc. 8th Nobel Symposium Stockholm 1968, ed. N. Svartholm (Almqvist and Wiksells, Stockholm 1968) p.367; H.D. Politzer, Phys. Rep. 14 (1974) 129.

- [2] P.W. Higgs, Phys. Lett 12 (1964)132, Phys. Rev. Lett. 13 (1964)508; Phys.Rev. 145 (1966)1156; F.Englert and R.Brout, Phys. Rev. Lett. 13 (1964)321; G.S. Guralnik, C.R.Hagen and T.W.B. Kibble, Phys. Rev. Lett. 13 (1964)585; T.W.B. Kibble, Phys. Rev. 155 (1967)1554.
- [3] H. E. Haber, G. L. Kane, Phys. Rep. 117(1985) 75.
- [4] J. Gunion, H. Haber, G. Kane and S. Dawson, The Higgs Hunter's Guide (Addison-Wesley, Reading 1990).
- [5] K.A. Assamagan, et al., 'The Higgs Working Group: Summary Report', Report of the Higgs working group for the Workshop 'Physics at TeV Colliders', Les Houches, France 8-18 June 1999, hep-ph/0002258 and the references therein.
- [6] N. G. Deshpande, X. Tata and D. A. Dicus, Phys. Rev. **D29** 1527 (1984); E. Eichten, I. Hinchliffe, K. Lane and C. Quigg, Phys. Mod. Rev. **56**, 579 (1984); **58**, 1065(E) (1986).
- [7] S.S.D. Willenbrock, Phys. Rev. **35**,173 (1987); Y. Jiang, W.G. Ma, L. Han, M. Han and Z.H. Yu, J. Phys. **G24**, 83 (1998); A. Krause, T. Plehn, M. Spira and P.M. Zerwas, Nucl. Phys. **B519** 85 (1998); Barrientos Bendezu and B.A. Kniehl, Nucl. Phys. **B568** (2000)305; O. Brein, W. Hollik, Eur. Phys. J. **C13** (2000)175.
- [8] J.F.Gunion, H.E. Haber, F.E. Paige, W.-K. Tung and S.S.D. Willenbrock, Nucl. Phys. **B294** (1987) 621.
- [9] J.L. Diaz-Cruz and O.A. Sampayo, Phys. Rev. **D50**, (1994)6820.
- [10] S. Moretti and K. Odagiri, Phys. Rev. **D55**, (1997)5627.
- [11] D.A. Dicus, J.L. Hewett, C. Kao and T.G. Rizzo, Phys. Rev. **D40**, 789 (1989); A.A. Barrientos Bendezu and B.A. Kniehl, Phys. Rev. **D59** (1998)015009; Phys. Rev. **D61**, (2000)097701.
- [12] F. Zhou, W.G. Ma, Y. Jiang, L. Han, and L.H. Wan, Phys. Rev. **D63** (2001)015002; O. Brein, S. Kanemura, W. Hollik, Phys. Rev. **D63** (2001)015009.

- [13] Y.S. Yang, C.S. Li, L.G. Jin and S.H. Zhu, Phys.Rev. D62 (2000) 095012; O. Brein, S. Kanemura, W. Hollik, hep-ph/0008308.
- [14] S. Komamiya, Phys. Rev. **D38** (1988) 2158; A. Brignole et al.in Proceedings of the Workshop on e^+e^- Collisions at 50 GeV The Physics Potential, ed. P.M. Zerwas, DESY 92-123; A.Djouadi, J. Kalinowski, P.M. Zerwas, *ibid* and Z. Phys. C57 (1993) 569.
- [15] A. Arhrib, M. Capdequi Peyranère and G. Moulataka, Phys. Lett. **B341** (1995) 313; Marco A. Diaz and Tonnis A. ter Veldhuis hep-ph/9501315, DPF94 Proceedings; J. Guasch, W. Hollik and A. Kraft KA-TP-19-1999, hep-ph/9911452.
- [16] A. Arhrib, and G. Moulataka, Nucl. Phys. **B558** (1999) 3, hep-ph/9808317.
- [17] D. Bowser-Chao, K. Cheung, and S. Thomas, Phys. Lett.**B315**, 399 (1993); W.G. Ma, C.S. Li and L. Han, Phys. Rev. **D53**, 1304 (1996). S.H. Zhu, C.S. Li and C.S. Gao, Phys. Rev. **D58** (1998)055007.
- [18] S. Kanemura, Eur. Phys. J. **C17** (2000)473; A. Arhrib, M. C. Peyranere, W. Hollik and G. Moulataka, Nucl. Phys. **B581** (2000)34.
- [19] M. Drees and S. P. Martin, MAD-PH-879, UM-TH-95-02, hep-ph/9504324.
- [20] A. Dabelstein, Z. Phys. **C 67** (1995) 495 and the references therein.
- [21] A. Denner, Fortschr. Phys. **41** (1993) 4, p306.
- [22] J. Rosiek, Phys. Rev.**D41** (1990) 3464.
- [23] J.A. Rasa, D. Garcia, J. Guasch, R.A. Jimenez and J. Sola, Eur. Phys. J. C2(1998) 373; M.C. Peyranere, Int. J. Mod. Phys. A14(1999) 429, hep-ph/9809324.
- [24] W. Beenakker, A. Denner, W. Hollik, R. Mertig, T. Sack, and D. Wackeroth, Nucl. Phys. **B411**, (1994) 344.
- [25] I.F. Ginzburg, G.L. Kotkin, V.G. Serbo and V.I. Telnov, Pis'ma ZHETF 34(1981)514; Nucl. Instr. Methods 205(1983)47.

- [26] R. Blankenbecler and S.D. Drell, Phys. Rev. Lett. 61(2324)1988; F. Halzen, C.S. Kim and M.L. Stong, Phys. Lett. B274(489)1992; M. Drees and R.M. Godbole, Phys. Lett. 67(1189)1991.
- [27] V.Telnov, Nucl. Instr. Methods A294(72)1990.
- [28] D.E. Groom *et al.*, The European Physical Journal **C 15**, 1 (2000).
- [29] see for examples, J.R. Espinosa, and M Quiros, Phys. Lett **B266** (1991)389; K. Gunion and A. Turski, Phys. Rev. **D39** (1989)2701 and **D40**(1990)2333; M.Carena, M. Quiros and C.E.M. Wagner, Nucl. Phys.**B461**(1996)407.
- [30] P. Nath, R. Arnowitt and A.H. Chamseddine, "Applied N=1 Supergravity", World Scientific, Singapore, 1984.
- [31] Bernd A. Kniehl, Phys. Rep. 240(1994)211.
- [32] G. Passarino and M. Veltman, Nucl. Phys. **B160**,

Figure Captions

Fig.1 The Feynman diagrams of the subprocess $\gamma\gamma \rightarrow W^+H^-$, where the notations S^0 and S^+ denote neutral particles $h^0(H^0)$ and charged particles $H^+(W^+, G^+)$, respectively.

Fig.2 The diagrams contributing to self-energies of mixing $H^+ - W^-$ (Fig.2(1-2)) and $H^+ - G^-$ (Fig.2(3-5)).

Fig.3 Total cross sections of $e^+e^- \rightarrow \gamma\gamma \rightarrow W^\pm H^\mp$ in mSUGRA scenario as function of m_{H^\pm} with $\sqrt{s} = 1 \text{ TeV}$ in non-SUSY THDM and the MSSM.

Fig.4a Total cross sections of $e^+e^- \rightarrow \gamma\gamma \rightarrow W^\pm H^\mp$ in mSUGRA scenario as function of $\tan\beta$ with $\sqrt{s} = 1000 \text{ GeV}$ in non-SUSY THDM and the MSSM.

Fig.4b Total cross sections of $e^+e^- \rightarrow \gamma\gamma \rightarrow W^\pm H^\mp$ in mSUGRA scenario as function of $\tan\beta$ with $\sqrt{s} = 500 \text{ GeV}$ in non-SUSY THDM and the MSSM.

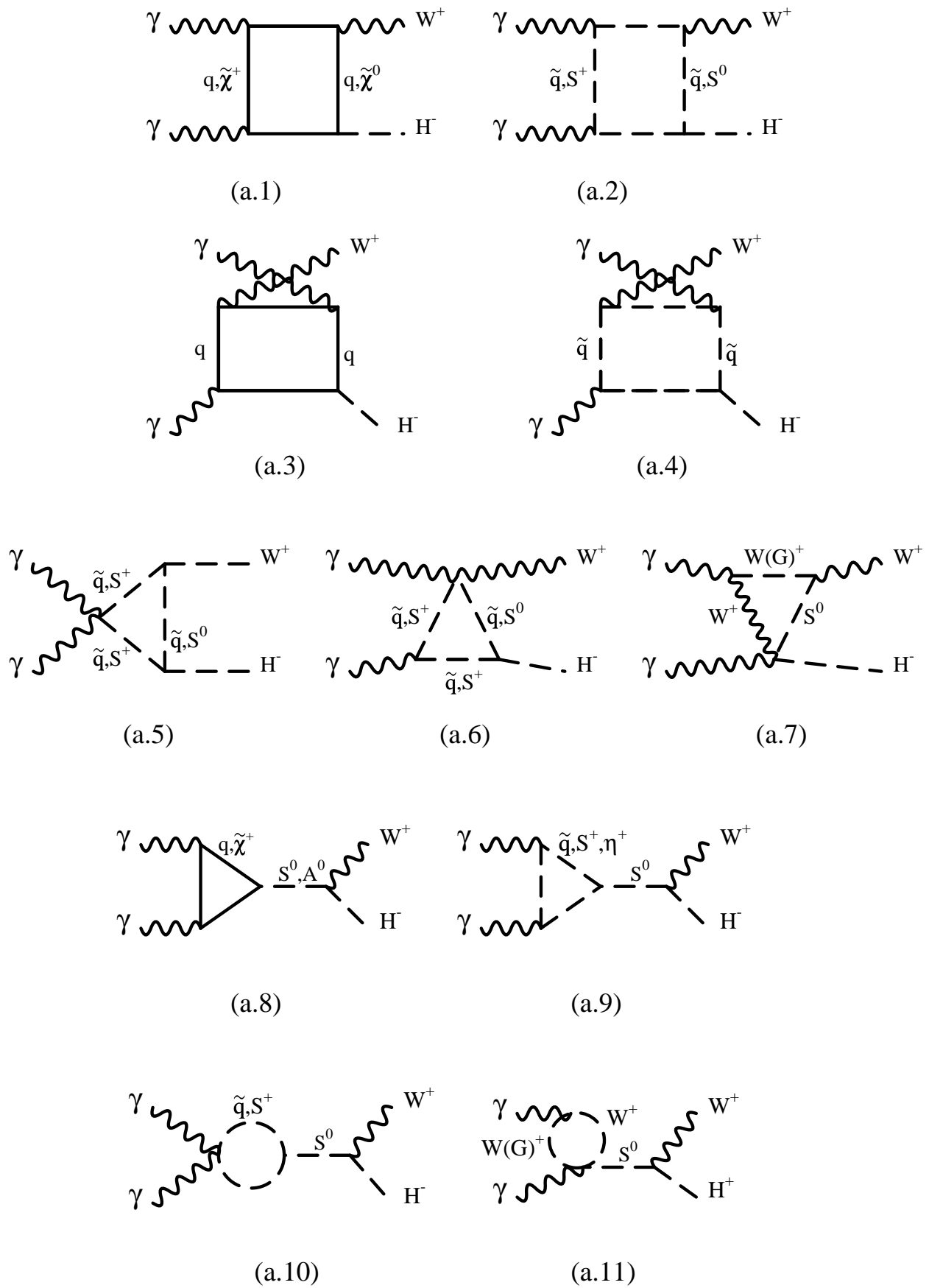
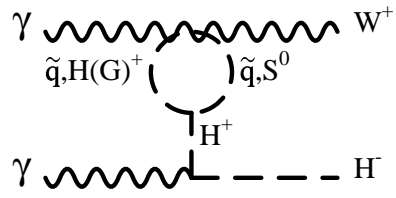
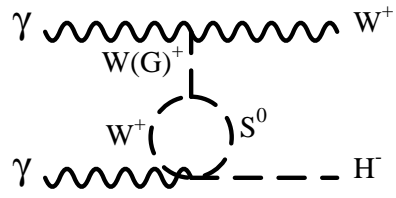


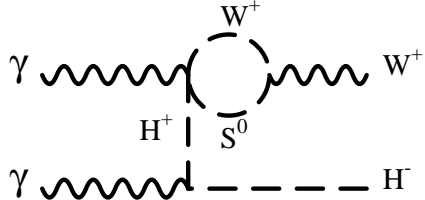
Fig.1



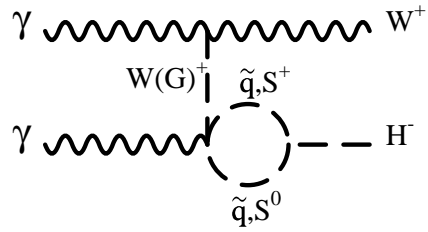
(a.12)



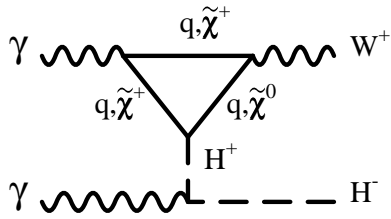
(a.13)



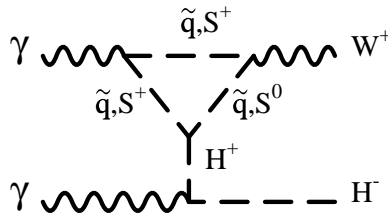
(a.14)



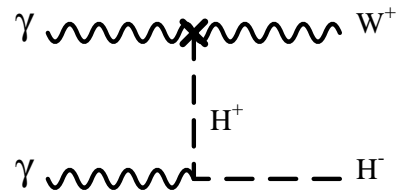
(a.15)



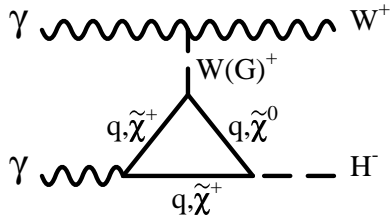
(a.16)



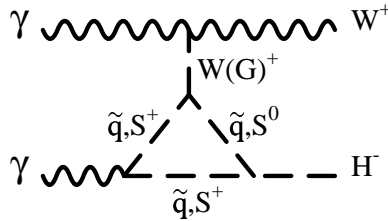
(a.17)



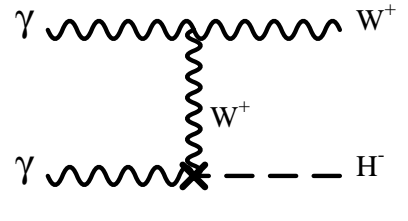
(b.1)



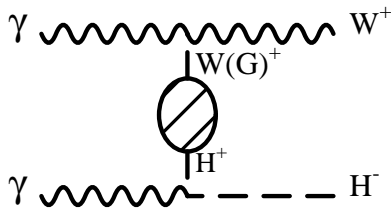
(a.18)



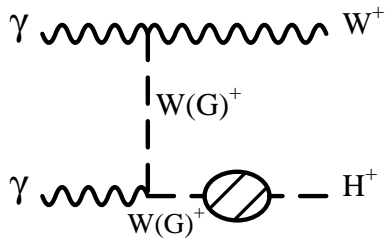
(a.19)



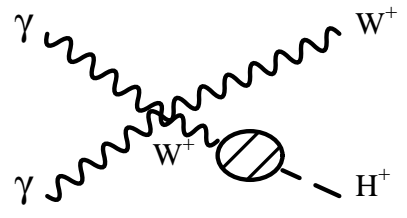
(b.2)



(b.3)



(b.4)



(b.5)

Fig.1(continued)

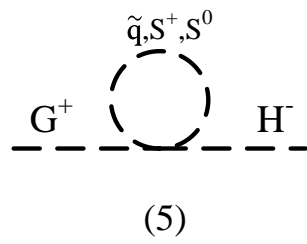
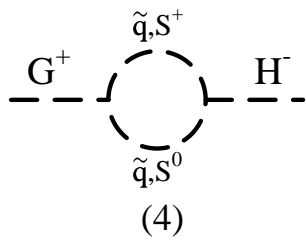
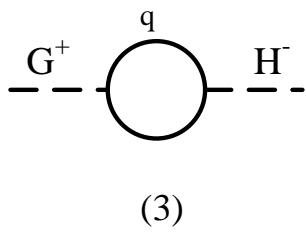
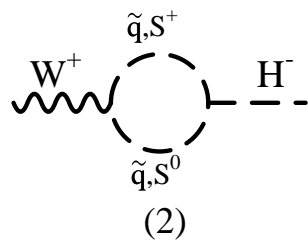
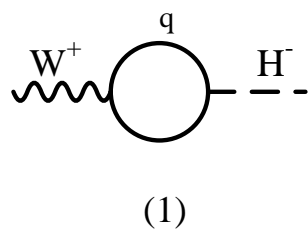


Fig.2

Fig. 3

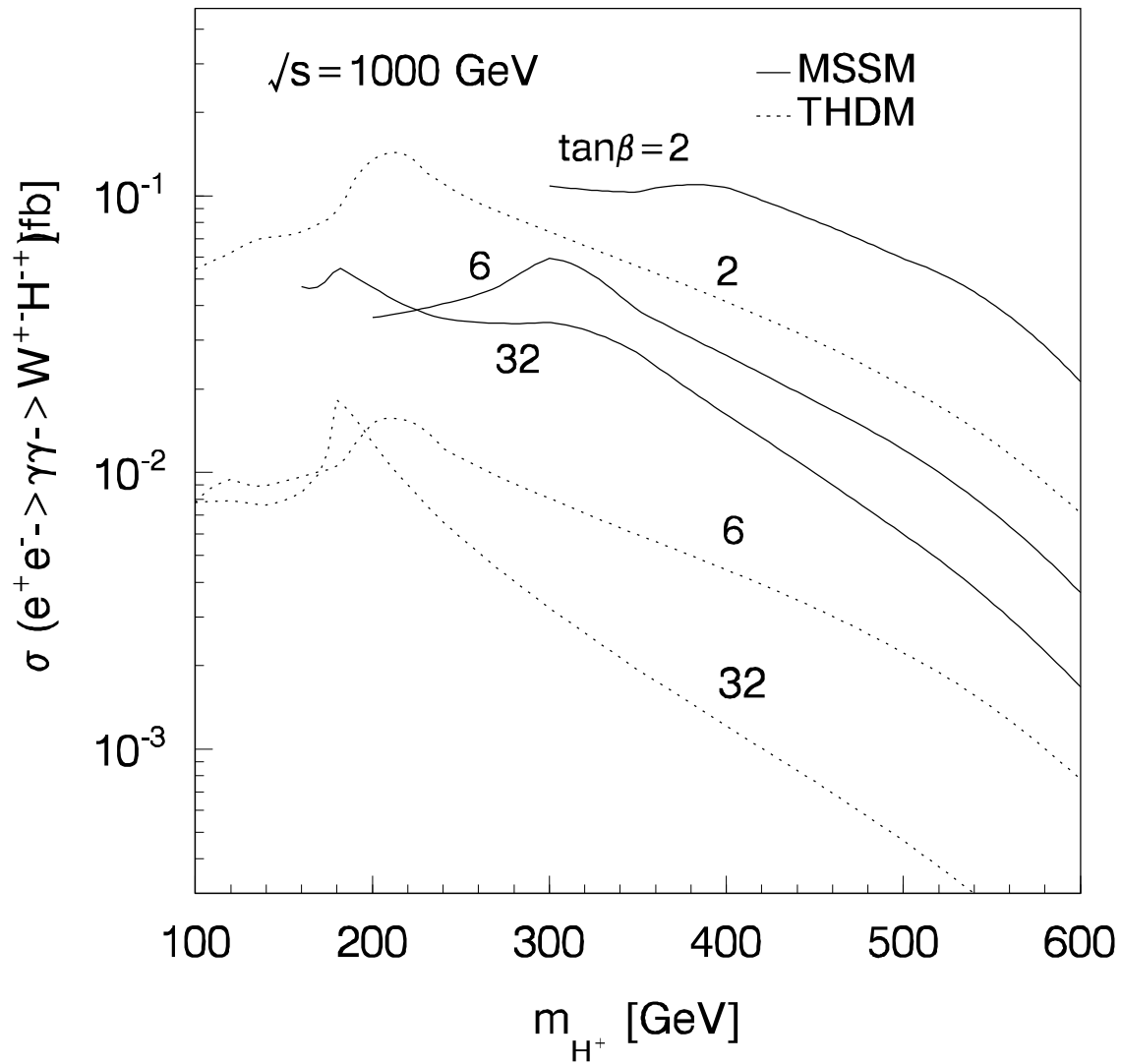


Fig. 4a

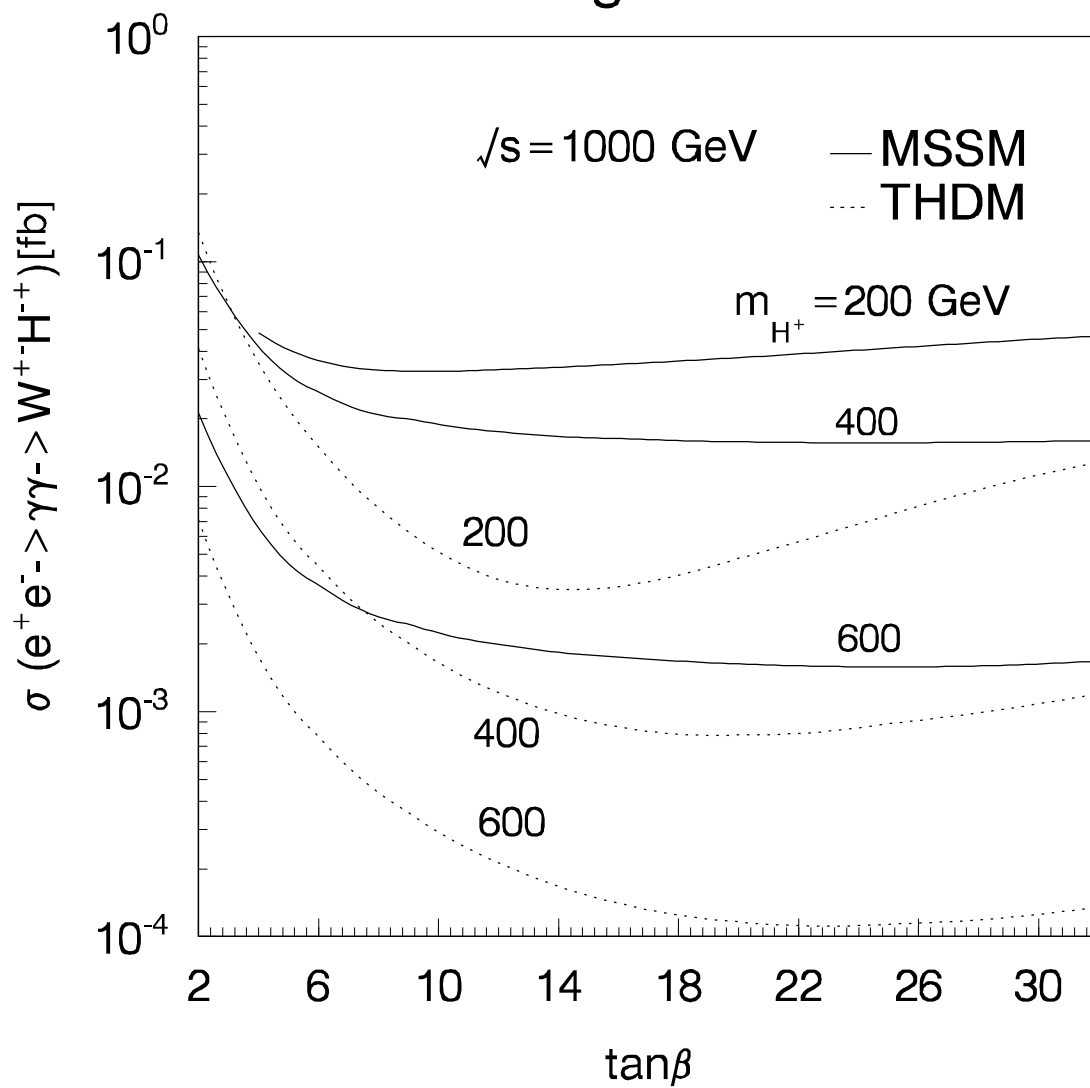


Fig. 4b

